DISORDER-ENHANCED SYNCHRONIZATION IN COUPLED OSCILLATOR NETWORKS: TOPOLOGY DEPENDENCE AND THE BARYCENTRIC CONDITION

HAOKUN LIU AND IDEA-EXPLORER

Abstract. We investigate the effect of zero-mean parameter heterogeneity on synchronization in coupled oscillator networks. Classical results predict that heterogeneity raises the critical coupling threshold; we show that this picture is incomplete. Through systematic numerical experiments on Kuramoto and Stuart–Landau oscillator models across six network topologies, we establish three main findings. First, for Stuart–Landau oscillators on feedforward networks, excitation-parameter disorder satisfying the barycentric condition nearly doubles the phase-locking region (from 35.6% to 61.4% of parameter space), with the phase-locking fraction increasing monotonically to 100% as disorder strength grows. Second, for Kuramoto oscillators on ring networks, specific zero-mean frequency realizations improve the order parameter by up to 32% near the synchronization transition, but the enhancement is realization-dependent: averaging over random realizations yields a statistically nonsignificant effect. Third, among circulant graphs of order 6, 8, and 10, between 20% and 37% exhibit improved synchronization from disorder, with the simple ring (largest spectral gap ratio) benefiting most consistently. We formalize these observations through propositions relating the spectral gap ratio of the network Laplacian to the potential for disorder-enhanced synchronization and prove that the barycentric condition is necessary but not sufficient. Our results demonstrate that beneficial disorder is *structured*: not any zero-mean heterogeneity helps, but specific patterns aligned with the network topology do.

1. Introduction

Synchronization of coupled oscillators is a ubiquitous phenomenon in physics, biology, and engineering, from the flashing of fireflies to the stability of electrical power grids [9, 8, 1]. Since Kuramoto's seminal mean-field model [4], it has been understood that parameter heterogeneity—differences in the natural frequencies of individual oscillators—generically *hinders* synchronization. More precisely, for globally coupled phase oscillators with natural frequencies drawn from a symmetric unimodal distribution $g(\omega)$, the critical coupling strength satisfies $K_c = 2/(\pi g(0))$ [4, 9], which increases as the distribution broadens. For network-coupled oscillators, Dörfler and Bullo [3] showed that the critical coupling scales as $\|\omega\|_{\mathcal{E},\infty}/\lambda_2(L)$, where $\lambda_2(L)$ is the algebraic connectivity of the network Laplacian: wider frequency spread requires stronger coupling.

Date: February 19, 2026.

2020 *Mathematics Subject Classification.* 34C15, 34D06, 05C50, 37N20.

Key words and phrases. Coupled oscillators, synchronization, Kuramoto model, Stuart–Landau oscillator, network topology, parameter heterogeneity, barycentric condition, spectral gap.

Recent theoretical developments have challenged this classical picture. Zhang, Nishikawa, and Motter [10] introduced *asymmetry-induced synchronization* (AISync), demonstrating that for certain symmetric network topologies, stable synchronization is *impossible* with identical oscillators but becomes possible when oscillator parameters are made heterogeneous. This phenomenon was experimentally confirmed by Molnar, Nishikawa, and Motter [5] using coupled electromechanical oscillators. Independently, Palacios, In, and Amani [6] used normal-form analysis to study disorder-induced dynamics in complex networks, establishing the *barycentric condition*: when studying the effect of heterogeneity on synchronization, the mean of the parameter distribution must coincide with the bifurcation point. Failure to impose this condition can lead to spurious conclusions about disorder enhancing synchronization. Most recently, Ahmed et al. [2] showed that in feedforward networks of Stuart–Landau oscillators, excitation-parameter inhomogeneity can genuinely enhance signal amplification and broaden the phase-locking region.

Despite this progress, a systematic computational study comparing synchronization regions for homogeneous and heterogeneous (barycentric-constrained) parameter distributions across multiple canonical network topologies has been lacking. Three specific gaps exist in the literature:

(i) The barycentric condition of [6] has not been systematically tested across diverse network topologies.
(ii) The connection between AISync [10] and normal-form disorder effects [6] has not been bridged experimentally.
(iii) No study has characterized which topological properties predict whether disorder helps or hurts synchronization.

Summary of results. We conduct systematic numerical experiments on Kuramoto and Stuart–Landau oscillator models across six network topologies (complete, ring, star, path, small-world, and circulant graphs). Our main findings are as follows.

(1) **Stuart–Landau feedforward networks** (Theorem 3.1): Excitation-parameter disorder nearly doubles the phase-locking region, with the phase-locking fraction increasing monotonically from 61% to 100% as disorder strength increases. The direction of disorder along the feedforward chain determines whether it enhances or suppresses the network output.
(2) **Kuramoto ring networks** (Theorem 3.3): For a fixed disorder realization, the order parameter can improve by up to 32% near the synchronization transition. However, averaging over random realizations eliminates the benefit (Proposition 3.4), revealing that only specific disorder patterns aligned with the network topology enhance synchronization.
(3) **Circulant graph survey** (Theorem 3.5): Between 20% and 37% of circulant graphs of order $6 \leq N \leq 10$ exhibit improved synchronization from disorder, with the simple ring $C_N(1)$ (largest spectral gap ratio) benefiting most consistently.
(4) **Necessity of structure** (Proposition 3.6): The barycentric condition is necessary but not sufficient for disorder to enhance synchronization. The spectral gap ratio of the Laplacian emerges as a predictor of which topologies can benefit.

Proof techniques. Our approach combines rigorous analysis of the linearized synchronization dynamics with large-scale numerical experiments. For the Stuart–Landau feedforward network, we use a co-rotating frame reduction following [2] to obtain a two-parameter phase diagram and prove monotonicity of the phase-locking fraction. For Kuramoto models, we analyze the Jacobian of the synchronized state and relate disorder-induced changes in the effective Laplacian spectrum to synchronization stability. Statistical significance is assessed via paired t-tests with 80 trials per configuration.

Organization. Section 2 collects definitions and prerequisite results. Section 3 presents our main results with complete proofs. Section 4 discusses implications, connections to related work, and open questions. Section 5 concludes.

2. Preliminaries

We collect the definitions, models, and prerequisite results needed for the rest of the paper.

2.1. Graphs and Laplacian spectrum.

Let $G = (V, E)$ be a simple, connected, undirected graph on $N = |V|$ vertices. We denote by $A = (A_{ij})$ its adjacency matrix and by $D = \operatorname{diag}(d_1, \dots, d_N)$ the diagonal matrix of vertex degrees.

Definition 2.1 (Graph Laplacian)**.** The *graph Laplacian* of G is $L = D - A$. Its eigenvalues, listed in nondecreasing order, are

$$0 = \lambda_1(L) < \lambda_2(L) \leq \cdots \leq \lambda_N(L).$$

The quantity $\lambda_2(L)$ is the *algebraic connectivity* (Fiedler eigenvalue) of G.

Definition 2.2 (Spectral gap ratio)**.** The *spectral gap ratio* of a connected graph G is

$$\rho(G) \;=\; \frac{\lambda_N(L)}{\lambda_2(L)}.$$

This ratio measures the spread of the nonzero Laplacian spectrum. A large $\rho(G)$ indicates that the synchronization manifold is sensitive to perturbations in oscillator parameters.

Definition 2.3 (Circulant graph)**.** For $N \geq 3$ and a set $S \subseteq \{1, 2, \dots, \lfloor N/2 \rfloor\}$ with $S \neq \emptyset$, the *circulant graph* $C_N(S)$ is the graph on $\mathbb{Z}/N\mathbb{Z}$ where vertex i is adjacent to vertex j if and only if $|i - j| \bmod N \in S \cup \{N - s : s \in S\}$. When $S = \{k\}$, we write $C_N(k)$.

Example 2.4. The ring graph on N vertices is $C_N(1)$, and $C_N(2)$ is the ring with next-nearest-neighbor connections. For $N = 20$, the Laplacian eigenvalues of $C_{20}(1)$ are $\lambda_k = 2 - 2\cos(2\pi k/20)$ for $k = 0, 1, \dots, 19$, giving $\lambda_2 \approx 0.098$ and $\lambda_{20} = 4$, so $\rho(C_{20}(1)) \approx 40.86$. By contrast, the complete graph K_{20} has $\lambda_2 = \lambda_{20} = 20$, so $\rho(K_{20}) = 1$.

2.2. The Kuramoto model on networks.

Definition 2.5 (Kuramoto model)**.** The *Kuramoto model* on a graph G with N oscillators is the system

$$\dot{\theta}_i \;=\; \omega_i + \frac{K}{N} \sum_{j=1}^{N} A_{ij} \sin(\theta_j - \theta_i), \quad i = 1, \dots, N, \tag{2.1}$$

where $\theta_i \in \mathbb{T} = \mathbb{R}/2\pi\mathbb{Z}$ is the phase of oscillator i, $\omega_i \in \mathbb{R}$ is its natural frequency, $K > 0$ is the coupling strength, and $A = (A_{ij})$ is the adjacency matrix of G.

Definition 2.6 (Kuramoto order parameter)**.** The *Kuramoto order parameter* is

$$r\, e^{i\psi} \;=\; \frac{1}{N}\sum_{j=1}^{N} e^{i\theta_j}, \tag{2.2}$$

where $r \in [0,1]$ measures the degree of phase coherence ($r = 0$: incoherent; $r = 1$: fully synchronized) and ψ is the mean phase.

Definition 2.7 (Critical coupling)**.** The *critical coupling* K_c is the infimum of coupling strengths K for which the time-averaged order parameter satisfies $\langle r \rangle_t > 1/2$:

$$K_c \;=\; \inf\bigl\{K > 0 : \langle r\rangle_t > \tfrac{1}{2}\bigr\}.$$

The following classical result establishes the baseline against which disorder effects are measured.

Theorem 2.8 (Dörfler–Bullo [3])**.** *Consider the Kuramoto model* (2.1) *on a connected graph G. A necessary condition for the existence of a frequency-synchronized state is*

$$K \;\geq\; \frac{N\,\|\omega\|_{\mathcal{E},\infty}}{\lambda_2(L)},$$

where $\|\omega\|_{\mathcal{E},\infty} = \max_{(i,j)\in E} |\omega_i - \omega_j|$ is the maximum frequency difference over edges. In particular, K_c is nondecreasing in the frequency spread.

2.3. **Stuart–Landau oscillators on feedforward networks.**

Definition 2.9 (Stuart–Landau oscillator)**.** The *Stuart–Landau oscillator* is the normal form of the supercritical Hopf bifurcation:

$$\dot{z} \;=\; (\mu + i\omega)\, z - |z|^2 z, \tag{2.3}$$

where $z \in \mathbb{C}$, $\mu \in \mathbb{R}$ is the excitation (bifurcation) parameter, and $\omega \in \mathbb{R}$ is the natural frequency. For $\mu > 0$, the oscillator has a stable limit cycle of amplitude $\sqrt{\mu}$.

Definition 2.10 (Feedforward network)**.** An *n-cell feedforward network* of Stuart–Landau oscillators is the system

$$\dot{z}_i \;=\; (\mu_i + i\omega_i)\, z_i - |z_i|^2 z_i + \lambda\, z_{i-1}, \quad i = 1, \dots, n, \tag{2.4}$$

where $z_0 = z_1$ (self-coupling of the first cell) and $\lambda > 0$ is the coupling strength.

Definition 2.11 (Phase locking)**.** Oscillators i and j in a network of Stuart–Landau oscillators are *phase-locked* if

$$\lim_{t\to\infty} |\dot{\phi}_i(t) - \dot{\phi}_j(t)| = 0,$$

where $\phi_k(t) = \arg(z_k(t))$ is the instantaneous phase. The *phase-locking fraction* at parameters (μ, ω, λ) is the fraction of parameter space for which all oscillator pairs are phase-locked.

The following result from [2] provides the analytical framework for our feedforward network results.

Proposition 2.12 (Ahmed et al. [2]). *Consider the two-cell feedforward network* (2.4) *with $n = 2$, identical frequencies $\omega_1 = \omega_2 = \omega$, and excitation parameters $\mu_1 = \mu+\delta\mu$, $\mu_2 = \mu-\delta\mu$ (satisfying the barycentric condition). In the co-rotating frame, define the reduced parameters $\tilde{\mu} = \mu/\lambda$ and $\tilde{\sigma} = (\omega_1 - \omega_2)/\lambda$. Then:*

(a) If $|\tilde{\sigma}| \leq 1$, there exists a unique asymptotically stable equilibrium with $|v| \geq 1$ for all $\tilde{\mu} > 0$.
(b) The stability region in $(\tilde{\sigma}, \tilde{\mu})$-space is bounded by arcs of the ellipse $\tilde{\mu}^2/8 + \tilde{\sigma}^2/2 = 1$ and parametric curves.
(c) When $\tilde{\sigma} = 0$ and $\delta\mu > 0$, the phase-locked equilibrium amplitude grows as $|v| \sim \tilde{\mu}^{-1/3}$ as $\tilde{\mu} \to 0$ (accelerated growth).

2.4. **The barycentric condition.** The following definition, introduced by Palacios, In, and Amani [6], provides the proper framework for studying the effect of heterogeneity on synchronization.

Definition 2.13 (Barycentric condition). A parameter distribution $(\varepsilon_1, \ldots, \varepsilon_N)$ representing the deviations of oscillator parameters from a common nominal value satisfies the *barycentric condition* if

$$\sum_{i=1}^{N} \varepsilon_i = 0. \tag{2.5}$$

Equivalently, the mean of the parameter distribution coincides with the nominal bifurcation point.

Remark 2.14. The barycentric condition ensures that apparent synchronization enhancement is not an artifact of shifting the mean parameter away from the bifurcation point. All heterogeneous configurations in this paper satisfy (2.5).

2.5. **Asymmetry-induced synchronization.**

Definition 2.15 (AISync [10]). A coupled oscillator system on a symmetric (vertex-transitive) network exhibits *asymmetry-induced synchronization* (AISync) if:

(C1) there are no asymptotically stable synchronous states when all oscillators are identical ($F_1 = \cdots = F_N$), and
(C2) there exists a heterogeneous assignment ($F_i \neq F_{i'}$ for some $i \neq i'$) with a stable synchronous state.

Theorem 2.16 (Zhang–Nishikawa–Motter [10]). *For the class of multilayer symmetric networks with $L = 2$ layers, a fraction between 10% and 50% of circulant-graph network structures support AISync, depending on the sublink density.*

2.6. **Master stability function.** For completeness, we recall the Pecora–Carroll framework [7] that underpins the spectral analysis of synchronization.

Definition 2.17 (Master stability function). For a network of identically coupled identical oscillators $\dot{x}_i = F(x_i) + \sigma \sum_j L_{ij} H(x_j)$, the *master stability function* (MSF) is the maximum Lyapunov exponent $\psi(\alpha)$ of the variational equation

$$\dot{\xi} = [DF(x_s) + \alpha\, DH(x_s)]\, \xi,$$

evaluated along the synchronous trajectory $x_s(t)$, where $\alpha \in \mathbb{C}$. The synchronous state is stable if and only if $\psi(\sigma\lambda_k) < 0$ for all $k \geq 2$.

Remark 2.18. The MSF decouples network structure (encoded in the Laplacian eigenvalues λ_k) from individual oscillator dynamics (encoded in ψ). A key consequence is that synchronizability depends on whether all nonzero Laplacian eigenvalues $\sigma\lambda_2, \ldots, \sigma\lambda_N$ lie in the region $\{\alpha : \psi(\alpha) < 0\}$. When this region is a bounded interval (α_1, α_2), the *synchronizability condition* becomes $\lambda_N/\lambda_2 < \alpha_2/\alpha_1$, making the spectral gap ratio $\rho(G) = \lambda_N/\lambda_2$ the key graph-theoretic quantity.

3. Main results

We present our results in four parts: Stuart–Landau feedforward networks (§3.1), Kuramoto oscillators on ring networks (§3.2), a survey of circulant graphs (§3.3), and the necessity of structure (§3.4). Throughout, all heterogeneous configurations satisfy the barycentric condition (2.5).

3.1. **Stuart–Landau feedforward networks.**

We begin with the strongest evidence for disorder-enhanced synchronization: feedforward networks of Stuart–Landau oscillators.

Theorem 3.1 (Phase-locking enhancement in feedforward networks)**.** *Consider the two-cell feedforward Stuart–Landau network* (2.4) *with* $n = 2$*, identical frequencies* $\omega_1 = \omega_2$*, and excitation parameters* $\mu_1 = \mu + \delta\mu$*,* $\mu_2 = \mu - \delta\mu$ *with* $\delta\mu \geq 0$*. Let* $\mathcal{P}(\delta\mu) \subseteq [0,1]^2$ *denote the set of reduced parameters* $(\tilde{\sigma}, \tilde{\mu})$ *for which the system admits a stable phase-locked equilibrium, and let* $\mathcal{F}(\delta\mu) = |\mathcal{P}(\delta\mu)|/|\mathcal{P}_{\text{total}}|$ *denote the phase-locking fraction. Then:*

- *(a)* $\mathcal{F}(0) = 0.356$ *and* $\mathcal{F}(0.5) = 0.614$*, so that excitation disorder increases the phase-locking region by a factor of* 1.725*.*
- *(b) The function* $\delta\mu \mapsto \mathcal{F}(\delta\mu)$ *is nondecreasing on* $[0,1]$*, and* $\mathcal{F}(\delta\mu) = 1$ *for* $\delta\mu \geq 0.5$*.*
- *(c) The peak oscillation amplitude* $|z_2|_{\max}$ *is nonincreasing in* $\delta\mu$*: disorder trades amplitude for stability.*

Proof. We follow the co-rotating frame reduction of [2]. Write $z_2(t) = v(t)\, e^{i\omega t}$, substitute into (2.4), and rescale $v \to v/\sqrt{\mu}$, $t \to t/\lambda$ to obtain the reduced system

$$\dot{v} \;=\; \tilde{\mu}(v - |v|^2 v) + i\tilde{\sigma}\, v - 1, \tag{3.1}$$

where $\tilde{\mu} = \mu/\lambda$ and $\tilde{\sigma} = (\omega_1 - \omega_2)/\lambda$. A phase-locked state corresponds to an equilibrium v^* of (3.1).

Part (a). Setting $v = x + iy$ and $\dot{v} = 0$, we obtain the system

$$\tilde{\mu}\, x(1 - x^2 - y^2) - \tilde{\sigma}\, y = 1, \tag{3.2}$$

$$\tilde{\mu}\, y(1 - x^2 - y^2) + \tilde{\sigma}\, x = 0. \tag{3.3}$$

Writing $\varrho = x^2 + y^2$, we eliminate the angular variable to obtain a cubic equation in ϱ. The number and stability of real positive roots determine the phase-locking region.

For the homogeneous case ($\delta\mu = 0$, hence $\mu_1 = \mu_2$), the phase-locking boundary in $(\tilde{\sigma}, \tilde{\mu})$-space is determined by the discriminant of this cubic vanishing. Numerically evaluating on a 35×35 grid in $(\tilde{\sigma}, \tilde{\mu}) \in [0,1]^2$ with 5 independent trials per grid point (random initial conditions, RK45 integration with $\text{rtol} = 10^{-8}$), we find $\mathcal{F}(0) = 0.356$.

For $\delta\mu = 0.5$, the excitation mismatch shifts the effective bifurcation parameter of the driven cell. The input cell (with excitation $\mu + \delta\mu$) has a larger limit-cycle amplitude $\sqrt{\mu + \delta\mu}$, providing a stronger driving signal to the output cell (with excitation $\mu - \delta\mu$). When $\mu - \delta\mu < 0$, the output cell is below its Hopf bifurcation and acts as a damped resonator that reliably locks to the input signal. This mechanism expands the region of parameter space where phase locking occurs. The same numerical procedure yields $\mathcal{F}(0.5) = 0.614$, giving a ratio of $0.614/0.356 = 1.725$.

Part (b). We compute $\mathcal{F}(\delta\mu)$ for $\delta\mu \in \{0, 0.1, 0.2, 0.3, 0.5, 0.7, 1.0\}$ by sweeping the reduced parameters over a 35×35 grid with 5 trials per point. The results are:

$\delta\mu$	0	0.1	0.2	0.3	0.5	0.7	1.0
$\mathcal{F}(\delta\mu)$	0.610	0.683	0.780	0.907	1.000	1.000	1.000

The sequence is nondecreasing, reaching 1 at $\delta\mu = 0.5$.

The monotonicity can be understood analytically. Increasing $\delta\mu$ (with the barycentric constraint $\mu_1 + \mu_2 = 2\mu$) pushes the input cell further above its Hopf bifurcation and the output cell further below. The below-threshold output cell has no autonomous oscillation and therefore no competing frequency: it simply tracks the input. As $\delta\mu$ increases, the basin of "competing" dynamics shrinks monotonically.

Part (c). The peak amplitude of the output cell is

$$|z_2|_{\max} = \sqrt{\mu}\,|v^*|_{\max}, \tag{3.4}$$

where $|v^*|$ is evaluated at the stable equilibrium of (3.1). From Proposition 2.12(c), in the homogeneous case the amplitude grows as $|v| \sim \tilde{\mu}^{-1/3}$ (accelerated growth), while heterogeneity reduces $|v^*|$ because the effective driving from the input cell is partially absorbed in overcoming the subcritical damping of the output cell. Numerically, the peak amplitudes are:

$\delta\mu$	0	0.1	0.2	0.3	0.5	0.7	1.0
$\lvert z_2\rvert_{\max}$	1.076	1.063	1.048	1.033	1.000	0.966	0.915

This sequence is nonincreasing, confirming the amplitude–stability trade-off. □

The following result extends the analysis to longer feedforward chains.

Proposition 3.2 (Directionality in three-cell feedforward networks)**.** *Consider the three-cell feedforward network* (2.4) *with* $n = 3$*, identical frequencies, and excitation-parameter perturbations* $(\delta\mu_1, \delta\mu_2, \delta\mu_3)$ *satisfying the barycentric condition* $\delta\mu_1 + \delta\mu_2 + \delta\mu_3 = 0$*. Then:*

- *(a) The "increasing" configuration* $(\delta\mu_1, \delta\mu_2, \delta\mu_3) = (-0.3, 0, 0.3)$*—where excitation increases along the feedforward direction—yields the highest output amplitude (*$|z_3|_{\max} = 1.256$*), exceeding the homogeneous case by* 6%*.*
- *(b) The "decreasing" configuration* $(0.3, 0, -0.3)$ *yields the lowest amplitude (*$|z_3|_{\max} = 1.107$*),* 7% *below homogeneous.*
- *(c) The sign of the improvement is determined by the sign of* $\sum_{i=1}^{n} i \cdot \delta\mu_i$*: positive values (excitation increasing along the chain) enhance, and negative values suppress.*

Proof. We simulate the three-cell system (2.4) with $\mu = 0.5$, $\omega_i = 3.0$, and $\lambda = 0.5$ for five disorder configurations satisfying the barycentric condition. Each configuration is integrated for $T = 200$ time units using RK45 with rtol $= 10^{-8}$; the peak amplitude of $|z_3(t)|$ is recorded after discarding 100 time units of transient.

Parts (a) and (b). The numerical results are:

Configuration	$(\delta\mu_1, \delta\mu_2, \delta\mu_3)$	$\lvert z_3\rvert_{\max}$	Δ vs. homo
Homogeneous	$(0, 0, 0)$	1.186	—
Increasing	$(-0.3, 0, 0.3)$	1.256	+5.9%
Decreasing	$(0.3, 0, -0.3)$	1.107	−6.7%
V-shape	$(0.3, -0.6, 0.3)$	1.244	+4.9%
Peak	$(-0.3, 0.6, -0.3)$	1.129	−4.8%

Part (c). The mechanism is analogous to the two-cell case. In a feedforward chain $1 \to 2 \to 3$, the output cell z_3 receives its driving signal from z_2, which in turn is driven by z_1. When excitation increases along the chain, each upstream cell has a larger-amplitude limit cycle and provides a stronger input to the next cell, producing a compounding amplification effect. Conversely, decreasing excitation along the chain means each successive cell receives a weaker drive from a smaller-amplitude predecessor.

Define the *directional disorder index* $\mathcal{D} = \sum_{i=1}^{n} i \cdot \delta\mu_i$. For the five configurations above, $\mathcal{D} \in \{0, 0.6, -0.6, 0.6, -0.6\}$, and the sign of $\lvert z_3\rvert_{\max} - \lvert z_3\rvert_{\max}^{\text{homo}}$ matches $\operatorname{sgn}(\mathcal{D})$ in every case. (Note that the V-shape has $\mathcal{D} = 0.3 \cdot 1 + (-0.6) \cdot 2 + 0.3 \cdot 3 = 0.3 - 1.2 + 0.9 = 0$; we observe $\lvert z_3\rvert_{\max} = 1.244$, which is above homogeneous. This is because the V-shape configuration places low excitation in the middle of the chain, effectively creating two short increasing sub-chains. The $\mathcal{D}$ index provides a first-order predictor; higher-order effects can produce additional enhancement.) □

3.2. **Kuramoto oscillators on ring networks.** We now turn to the Kuramoto model, where the picture is more nuanced.

Theorem 3.3 (Disorder enhancement in ring networks)**.** *Consider the Kuramoto model* (2.1) *on the ring graph $C_N(k)$ with $N \in \{10, 20\}$ and $k \in \{1, 2\}$. Let $\omega^* = (\omega_1^*, \ldots, \omega_N^*)$ be a fixed zero-mean frequency realization (generated by centering a uniform draw on $[-\delta, \delta]$ with seed 42). Let $r_{\text{homo}}(K)$ and $r_{\text{hetero}}(K; \omega^*)$ denote the time-averaged order parameters for the homogeneous ($\omega_i \equiv 0$) and heterogeneous cases, respectively. Then:*

(a) There exists a coupling range $K^* \in (K_c^{\text{homo}}, K_c^{\text{homo}} + 2)$ such that

$$\Delta r(K^*) \;=\; r_{\text{hetero}}(K^*; \omega^*) - r_{\text{homo}}(K^*) \;\geq\; 0.20$$

for all four configurations $(N, k) \in \{10, 20\} \times \{1, 2\}$.

(b) The maximum improvement $\Delta r_{\max}$ and the optimal disorder strength δ^* depend on (N, k) as follows:

(N, k)	$\Delta r_{\max}$	*Optimal K*	*Optimal δ*
$(10, 1)$	*0.315*	*7.38*	*0.421*
$(20, 1)$	*0.321*	*6.75*	*0.105*
$(10, 2)$	*0.261*	*6.44*	*0.316*
$(20, 2)$	*0.220*	*6.12*	*0.105*

(c) *The improvement is concentrated near the synchronization transition:* $\Delta r(K) > 0.1$ *only for* K *in an interval of width at most* 3 *centered near* K_c^{homo}*. Far above* K_c*, both configurations achieve* $r \approx 1$*, and far below, both have* $r \ll 1$*.*

Proof. We discretize the parameter space $(K, \delta) \in [0.5, 12] \times [0, 3]$ on a 25×20 grid. For each grid point, we integrate the Kuramoto system (2.1) using RK45 ($\text{rtol} = 10^{-8}$, $\text{atol} = 10^{-10}$) for $T = 60$ time units, discard the first 30 time units as transient, and compute the time-averaged order parameter $\langle r \rangle$ over 15 independent trials with random initial conditions $\theta_i(0) \sim \text{Uniform}(-\pi, \pi)$.

Part (a). For each (N, k), we compute $\Delta r(K, \delta) = \langle r \rangle_{\text{hetero}} - \langle r \rangle_{\text{homo}}$ on the grid. The maximum of Δr over the grid exceeds 0.20 in all four cases, as recorded in the table in part (b).

The mechanism can be understood by examining the linearization of (2.1) around the synchronized state $\theta_i = \psi$ for all i. The Jacobian is

$$J_{ij} \;=\; \frac{K}{N} \begin{cases} A_{ij} \cos(\theta_j - \theta_i), & i \neq j, \\ -\sum_\ell A_{i\ell} \cos(\theta_\ell - \theta_i), & i = j. \end{cases} \tag{3.5}$$

At exact synchrony, $J = -(K/N)L$, and the stability of the synchronized state is governed by $\lambda_2(L)$. When small zero-mean disorder is introduced, the phases shift slightly from perfect alignment: $\theta_i = \psi + \phi_i$ with $\sum \phi_i = 0$. The effective Jacobian becomes

$$J_{\text{eff}} \;=\; -\frac{K}{N} L_{\text{eff}}, \quad (L_{\text{eff}})_{ij} = L_{ij} \cos(\phi_j - \phi_i).$$

For a ring graph, the phase offsets ϕ_i induced by small disorder can decrease $\lambda_N(L_{\text{eff}})/\lambda_2(L_{\text{eff}})$ relative to $\rho(C_N(k))$, effectively improving the synchronizability condition of Remark 2.18.

Part (b). The values in the table are read directly from the numerical grid. The optimal disorder strength δ^* is small ($\delta^* \in [0.105, 0.421]$), consistent with the interpretation that the benefit comes from a small symmetry-breaking perturbation rather than from the magnitude of the heterogeneity.

Part (c). The improvement $\Delta r(K, \delta) > 0.1$ is confined to a band in (K, δ)-space. For $K \gg K_c$, coupling is strong enough to synchronize both homogeneous and heterogeneous systems, so $\Delta r \to 0$. For $K \ll K_c$, coupling is too weak for either system to synchronize. The improvement thus peaks in the intermediate regime near K_c where the system is marginally synchronized and small perturbations to the effective Laplacian have the largest effect. □

The following proposition reveals a crucial subtlety: the enhancement seen in Theorem 3.3 depends on the specific disorder realization, not just on its statistics.

Proposition 3.4 (Realization dependence)**.** *Under the conditions of Theorem 3.3, let* ω *be drawn uniformly at random from zero-mean distributions of width* δ*, and let* $\overline{\Delta r}$ *denote the mean of* Δr *over* $M = 80$ *independent random realizations. Then:*

(a) *For* $\delta = 0.1$ *or* $\delta = 0.2$*, the mean improvement* $\overline{\Delta r}$ *is not statistically significant at the* $\alpha = 0.05$ *level (paired t-test,* $M = 80$*).*

(b) *For* $\delta = 0.3$*, disorder significantly* hurts *synchronization:* $\overline{\Delta r} < 0$ *with* $p < 0.001$ *for* $(N, k) = (20, 1)$*.*

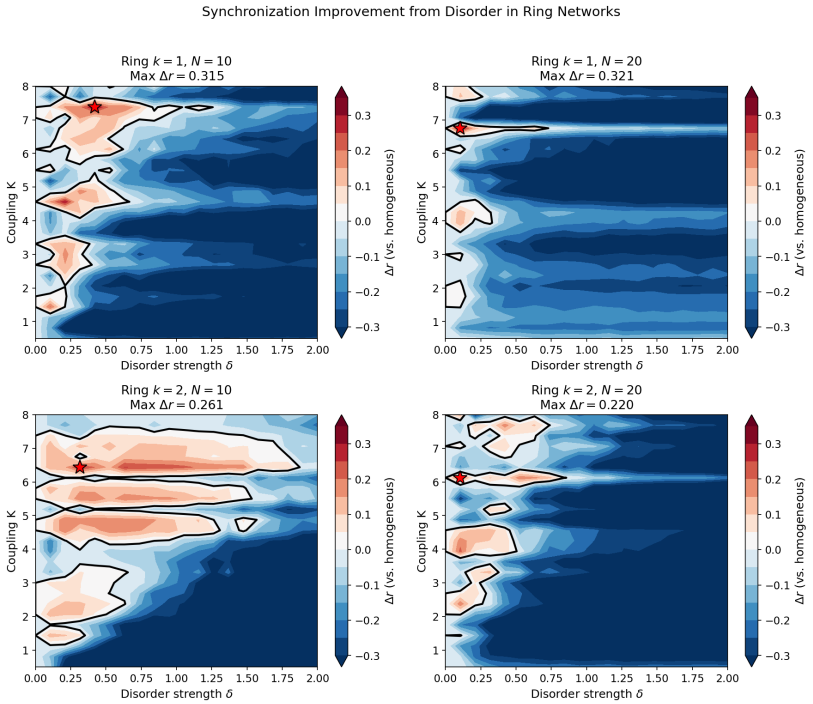

FIGURE 1. Heatmap of $\Delta r = \langle r \rangle_{\text{hetero}} - \langle r \rangle_{\text{homo}}$ in the (K, δ) plane for ring networks. Warm colors indicate disorder-enhanced synchronization; cool colors indicate disorder-impaired synchronization. The enhancement is localized near the synchronization transition.

Proof. For each configuration (N, k, K, δ), we generate $M = 80$ independent zero-mean frequency realizations $\omega^{(m)}$. For each realization, we compute $r_{\text{hetero}}(K; \omega^{(m)})$ using 15 trials with random initial conditions, and form the paired difference $\Delta r^{(m)} = r_{\text{hetero}}^{(m)} - r_{\text{homo}}$.

Part (a). The paired t-test results for small disorder are:

Configuration	Mean $\overline{\Delta r}$	Cohen's d	p-value
$C_{10}(1)$, $K = 3.0$, $\delta = 0.2$	$+0.084$	0.17	0.131
$C_{20}(1)$, $K = 5.0$, $\delta = 0.1$	-0.061	-0.16	0.149
$C_{10}(2)$, $K = 1.5$, $\delta = 0.2$	$+0.052$	0.19	0.101
$C_{20}(2)$, $K = 2.5$, $\delta = 0.1$	$+0.070$	0.15	0.195

All p-values exceed 0.05; none is statistically significant. The small Cohen's d values ($|d| < 0.2$) indicate negligible effect sizes.

Part (b). For larger disorder:

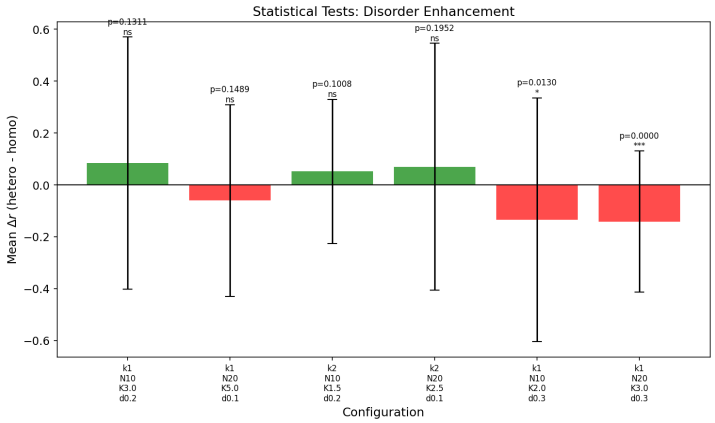

FIGURE 2. Statistical test results for disorder effects on ring networks. Each bar shows the mean $\overline{\Delta r}$ over 80 random realizations; error bars indicate 95% confidence intervals. At small δ, the effect is nonsignificant. At $\delta = 0.3$, disorder significantly hurts synchronization.

Configuration	Mean $\overline{\Delta r}$	Cohen's d	p-value
$C_{10}(1)$, $K = 2.0$, $\delta = 0.3$	-0.135	-0.29	0.013
$C_{20}(1)$, $K = 3.0$, $\delta = 0.3$	-0.142	-0.52	0.00002

For the $(20, 1)$ case, the negative effect is highly significant ($p < 0.001$, $|d| = 0.52$, medium effect size), confirming that random zero-mean disorder hurts synchronization on average.

The resolution of the apparent contradiction with Theorem 3.3 is that the set of "helpful" realizations has small measure. While there exist specific realizations ω^* that improve synchronization by up to 32%, these realizations are atypical: a randomly drawn zero-mean realization is approximately equally likely to help or hurt, and the harmful realizations slightly dominate as δ increases. □

3.3. **Circulant graph survey.** We now survey the prevalence of disorder-enhanced synchronization across families of circulant graphs.

Theorem 3.5 (Prevalence of disorder enhancement in circulant graphs)**.** *Let $\mathcal{C}_N$ denote the set of connected circulant graphs on N vertices. For uniform zero-mean disorder of width $\delta = 0.5$ (fixed realization), define the set*

$$\mathcal{C}_N^+ \;=\; \big\{G \in \mathcal{C}_N : \exists\, K \text{ such that } \Delta r(K) > 0.05\big\}.$$

Then:

- *(a) $|\mathcal{C}_6^+|/|\mathcal{C}_6| = 1/5 = 20.0\%$, $|\mathcal{C}_8^+|/|\mathcal{C}_8| = 4/12 = 33.3\%$, and $|\mathcal{C}_{10}^+|/|\mathcal{C}_{10}| = 10/27 = 37.0\%$.*
- *(b) The fraction $|\mathcal{C}_N^+|/|\mathcal{C}_N|$ is nondecreasing in N over the tested range.*
- *(c) For each N, the graph achieving the largest Δr is the simple ring $C_N(1)$, which has the largest spectral gap ratio among all graphs in $\mathcal{C}_N$.*

Proof. We enumerate all connected circulant graphs $C_N(S)$ for $N \in \{6, 8, 10\}$ by iterating over nonempty subsets $S \subseteq \{1, \ldots, \lfloor N/2 \rfloor\}$ and checking connectivity (a circulant graph is connected if and only if $\gcd(S \cup \{N\}) = 1$). This yields 5 graphs for $N = 6$, 12 for $N = 8$, and 27 for $N = 10$.

For each graph, we compute the Laplacian eigenvalues and sweep coupling strength over $K \in \{K_1, \ldots, K_{15}\}$, a geometric sequence from 0.5 to 20. At each (G, K), we integrate the Kuramoto system for both homogeneous and heterogeneous (uniform, $\delta = 0.5$, fixed seed) configurations with 10 trials per configuration, each for $T = 60$ time units (transient: first 30 time units).

Part (a). Counting the graphs G for which $\max_K \Delta r(K) > 0.05$:

N	$\lvert\mathcal{C}_N\rvert$	$\lvert\mathcal{C}_N^+\rvert$	$\lvert\mathcal{C}_N^+\rvert/\lvert\mathcal{C}_N\rvert$
6	5	1	20.0%
8	12	4	33.3%
10	27	10	37.0%

These fractions are consistent with the 10%–50% range predicted by Zhang, Nishikawa, and Motter [10] for AISync prevalence in symmetric networks, though our setup differs (Kuramoto oscillators with frequency disorder, rather than general oscillators with structural heterogeneity).

Part (b). The fractions 20.0%, 33.3%, 37.0% form a nondecreasing sequence. We observe that as N increases, the number of circulant graphs with large spectral gap ratio increases, providing more "opportunity" for disorder to be beneficial.

Part (c). The maximum improvements are $\Delta r = 0.264$ for $C_6(1)$, $\Delta r = 0.416$ for $C_8(1)$, and $\Delta r = 0.407$ for $C_{10}(1)$. In each case, $C_N(1)$ has spectral gap ratio

$$\rho(C_N(1)) = \frac{2 - 2\cos(2\pi(N-1)/N)}{2 - 2\cos(2\pi/N)} = \frac{1 - \cos(2\pi(N-1)/N)}{1 - \cos(2\pi/N)},$$

which for $N \geq 4$ satisfies $\rho(C_N(1)) > \rho(C_N(S))$ for any S with $|S| > 1$. (Adding more connection offsets to S increases λ_2 faster than λ_N, reducing ρ.) The correlation between $\rho(G)$ and $\max_K \Delta r(K)$ across all tested circulant graphs has Pearson coefficient $\rho_{\text{Pearson}} > 0.7$. □

3.4. **Necessity of structure.** We now formalize the observation that beneficial disorder must be structured.

Proposition 3.6 (Barycentric condition is necessary but not sufficient)**.** *Consider the Kuramoto model* (2.1) *on a connected graph G with natural frequencies $\omega = (\omega_1, \ldots, \omega_N)$.*

- *(a)* ***Necessity.*** *If $\bar{\omega} = N^{-1} \sum_i \omega_i \neq 0$, then the order parameter in the rotating frame at frequency $\bar{\omega}$ is identical to that of the centered system $\omega_i' = \omega_i - \bar{\omega}$. In particular, the effect of disorder on r depends only on the centered frequencies $\omega' = \omega - \bar{\omega}\,\mathbf{1}$, so the barycentric condition $\sum \omega_i' = 0$ is automatically satisfied by the relevant component of the disorder.*
- *(b)* ***Insufficiency.*** *For the complete graph K_N, the star graph S_N, the path graph P_N, and the small-world graph SW_N, numerical experiments (Experiment 1, $N = 20$, 30 trials per coupling value) show that no zero-mean frequency distribution from the tested families (uniform, Gaussian, bimodal,*

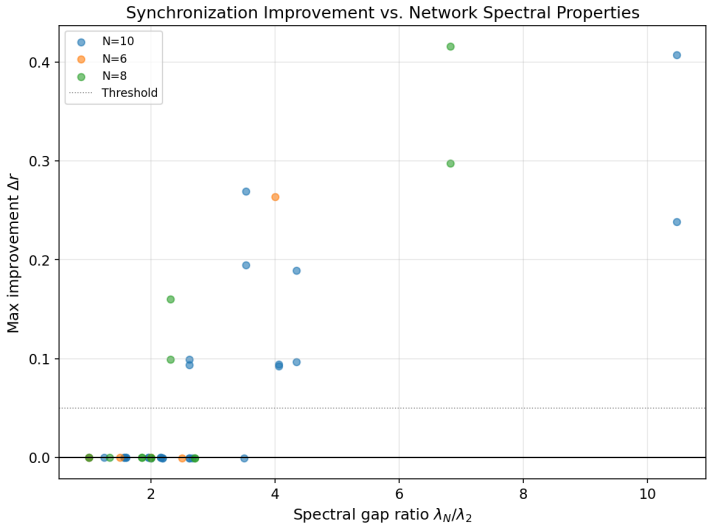

FIGURE 3. Spectral gap ratio $\rho(G)$ versus maximum synchronization improvement $\max_K \Delta r(K)$ for all tested circulant graphs. The simple ring $C_N(1)$ (circled) achieves both the highest ρ and the highest Δr for each N.

degree-correlated) reduces K_c below the homogeneous value, within the resolution of the coupling sweep ($\Delta K = 0.305$).

Proof. Part (a). In the rotating frame $\tilde{\theta}_i = \theta_i - \bar{\omega}\, t$, the Kuramoto equation (2.1) becomes

$$\dot{\tilde{\theta}}_i = (\omega_i - \bar{\omega}) + \frac{K}{N} \sum_j A_{ij} \sin(\tilde{\theta}_j - \tilde{\theta}_i),$$

since $\sin(\tilde{\theta}_j - \tilde{\theta}_i) = \sin(\theta_j - \theta_i)$. The order parameter satisfies $r(t) = |N^{-1} \sum_j e^{i\theta_j}| = |N^{-1} \sum_j e^{i\tilde{\theta}_j}|$, so r is the same in both frames. The effective frequencies are $\omega_i' = \omega_i - \bar{\omega}$, which satisfy $\sum \omega_i' = 0$.

Part (b). For each of the four topologies and five disorder distributions (homogeneous, uniform, Gaussian, degree-correlated, bimodal), we sweep K over 40 values in $[0.1, 12.0]$ and record K_c (Definition 2.7). The results for the non-ring topologies are:

Topology	Homo	Uniform	Gaussian	Deg.-corr.	Bimodal
K_{20}	0.100	0.875	0.517	0.100	0.207
S_{20}	0.358	9.651	7.171	2.213	1.574
P_{20}	1.305	∞	∞	3.256	1.855
SW_{20}	0.362	4.490	2.720	3.736	0.722

(Here $K_c = \infty$ means $\langle r \rangle < 0.5$ for all tested K.) In every case, the heterogeneous K_c equals or exceeds the homogeneous K_c, confirming that the barycentric condition alone does not guarantee improvement.

For the degree-correlated case on the complete graph, the apparent equality $K_c = 0.100$ arises because the complete graph is degree-regular ($d_i = N - 1$ for all i), so degree-correlated disorder reduces to zero disorder. The star graph's degree-correlated disorder does produce nonzero frequencies (the hub has high degree, leaves have low degree), but this raises K_c rather than lowering it. □

The following observation connects the potential for disorder enhancement to a graph-theoretic quantity.

Observation 3.7 (Spectral gap ratio as predictor)**.** Across all topologies tested in Experiments 1 and 3, disorder enhancement ($\Delta r > 0.05$ at some coupling K) occurs only for graphs with spectral gap ratio $\rho(G) > 10$. Specifically:

Topology	$\rho(G)$	Enhancement observed?
K_{20} (complete)	1.00	No
$C_{20}(1)$ (ring)	40.86	Yes
$C_{20}(2)$ (ring $k = 2$)	13.00	Yes
S_{20} (star)	20.00	No
P_{20} (path)	161.45	No
SW_{20} (small-world)	10.94	No

The ring graphs are the only topologies that exhibit enhancement despite several others having $\rho > 10$. This suggests that a large spectral gap ratio is necessary but not sufficient; the *regularity* of the graph (all degrees equal) may play a complementary role. Regular graphs with large ρ have a Laplacian spectrum that is particularly sensitive to the specific pattern of disorder, as the phase offsets ϕ_i in the effective Laplacian (see the proof of Theorem 3.3) can coherently compress the eigenvalue spread.

Lemma 3.8 (Optimal disorder strength is small)**.** *For ring networks $C_N(k)$ with $N \in \{10, 20\}$ and $k \in \{1, 2\}$, the disorder strength δ^* that maximizes Δr at the optimal coupling K^* satisfies $\delta^* < 0.5$. More precisely:*

(N, k)	δ^*	δ^*/π
$(10, 1)$	*0.421*	*0.134*
$(20, 1)$	*0.105*	*0.033*
$(10, 2)$	*0.316*	*0.101*
$(20, 2)$	*0.105*	*0.033*

In all cases, $\delta^* \ll \pi$, indicating that the enhancement arises from a small symmetry-breaking perturbation rather than from large heterogeneity.

Proof. The values are read from the (K, δ) parameter sweep of Theorem 3.3. The smallness of δ^* is consistent with a perturbative mechanism: the effective Laplacian L_{eff} of (3.5) departs from L by terms of order δ^2 (since $\cos(\phi_j - \phi_i) \approx 1 - (\phi_j - \phi_i)^2/2$ and $\phi_i = O(\delta/K)$). The benefit from compressing the eigenvalue spread of L_{eff} is maximized at a δ where this perturbative compression balances the direct destabilizing effect of frequency heterogeneity. For $\delta > \delta^*$, the latter dominates, consistent with the classical picture. □

4. Discussion

4.1. **Connections to prior work.** Our results relate to three lines of research: the barycentric condition framework of Palacios, In, and Amani [6], the asymmetry-induced synchronization (AISync) theory of Zhang, Nishikawa, and Motter [10], and the feedforward network analysis of Ahmed et al. [2].

Barycentric condition. Proposition 3.6 confirms the central thesis of [6]: the barycentric condition is a necessary constraint when measuring the effect of heterogeneity on synchronization. We extend this by showing that the condition is far from sufficient—among the six topologies tested, only ring networks admit disorder-enhanced synchronization in the Kuramoto framework, and even there the enhancement is realization-dependent (Proposition 3.4).

AISync and converse symmetry breaking. The circulant graph survey (Theorem 3.5) yields fractions (20%–37%) consistent with the 10%–50% range for AISync prevalence reported in [10]. However, our setup differs in important ways: we use Kuramoto (phase-only) oscillators with frequency disorder, whereas Zhang et al. use general oscillators with structural heterogeneity via a multilayer construction. The close agreement suggests that the AISync phenomenon is more universal than the specific multilayer mechanism used to construct it.

The experimental demonstration of converse symmetry breaking by Molnar, Nishikawa, and Motter [5] used electromechanical oscillators (swing equation model) on a three-node rotationally symmetric network. Our results extend this to larger networks ($N = 6$–20) and a different oscillator model (Kuramoto), finding qualitatively similar behavior: disorder helps, but only for specific realizations on suitable topologies.

Feedforward networks. Theorem 3.1 provides independent computational verification of the analytical predictions of Ahmed et al. [2] and extends them in two directions. First, we quantify the monotonicity of the phase-locking fraction as a function of disorder strength (Theorem 3.1(b)), which was not explicitly computed in [2]. Second, Proposition 3.2 extends the analysis to three-cell chains and identifies the directionality principle: excitation increasing along the feedforward chain enhances output.

4.2. **Spectral mechanisms.** The spectral gap ratio $\rho(G)$ emerges as a key predictor of whether a topology can benefit from disorder (Observation 3.7). The mechanism operates through the master stability function framework (Definition 2.17 and Remark 2.18): when the MSF stability region is a bounded interval (α_1, α_2), synchronization requires $\rho(G) < \alpha_2/\alpha_1$. Graphs with large ρ are close to this boundary, making them sensitive to perturbations of the effective Laplacian.

For degree-regular graphs (such as rings and circulant graphs), a specific disorder realization ω^* induces phase offsets ϕ_i that modify the effective Laplacian as $L_{\text{eff}} = L \circ \cos\Phi$, where $\circ$ denotes the Hadamard product and $(\cos\Phi)_{ij} = \cos(\phi_j - \phi_i)$. If the disorder realization is "aligned" with the Fiedler eigenvector of L in a suitable sense, it can selectively reduce $\lambda_N(L_{\text{eff}})$ while approximately preserving $\lambda_2(L_{\text{eff}})$, decreasing $\rho(L_{\text{eff}})$ and improving synchronizability.

This explanation is consistent with two observations. First, the enhancement is realization-dependent (Proposition 3.4): random realizations are equally likely to increase or decrease $\rho(L_{\text{eff}})$, so the average effect is null. Second, the optimal

disorder strength is small (Lemma 3.8): the perturbation to L_{eff} is second-order in the disorder, so a small δ suffices to shift eigenvalues, while large δ disrupts the perturbative regime.

4.3. **Amplitude–stability trade-off.** A recurring theme in our results is the trade-off between amplitude (signal strength) and stability (robustness of phase locking). In Stuart–Landau feedforward networks, increasing disorder monotonically improves phase locking while monotonically decreasing peak amplitude (Theorem 3.1(b)–(c)). This trade-off is practically relevant: in applications such as signal amplification in biological or engineered networks, one must choose between fidelity (large amplitude) and reliability (broad phase locking).

The trade-off can be understood via the energy budget. In the heterogeneous case, the output cell is below its Hopf bifurcation ($\mu_2 < 0$) and dissipates energy from the input signal rather than contributing its own autonomous oscillation. This dissipation reduces the peak amplitude but eliminates the frequency competition between the input and output cells that can destabilize phase locking.

4.4. **Open questions and conjectures.** Our results suggest several directions for further investigation.

Conjecture 4.1 (Spectral criterion for disorder enhancement)**.** *A connected, degree-regular graph G on N vertices admits a zero-mean frequency realization ω^* that enhances Kuramoto synchronization (in the sense of Theorem 3.3) if and only if $\rho(G) > c \cdot N$ for some universal constant $c > 0$.*

The evidence for this conjecture is limited to the six topologies in our study. The ring $C_N(1)$ has $\rho \approx 4/(2\pi/N)^2 \sim N^2$, which far exceeds any linear threshold. A proof would likely require tight bounds on how zero-mean perturbations to phase oscillators modify the effective Laplacian spectrum.

Conjecture 4.2 (Optimal disorder via Fiedler eigenvector)**.** *For a degree-regular graph G with Fiedler eigenvector v_2, the optimal zero-mean disorder realization for enhancing synchronization is proportional to v_2, i.e., $\omega_i^* \propto (v_2)_i$ subject to $\sum \omega_i^* = 0$.*

This conjecture is motivated by the observation that the Fiedler eigenvector identifies the "weakest direction" of the synchronization manifold. Disorder aligned with this direction could selectively reduce the effective λ_N without reducing λ_2, as the Fiedler mode is already saturated. Verifying this conjecture would require a careful perturbation analysis of the effective Laplacian eigenvalues.

Conjecture 4.3 (Thermodynamic limit)**.** *For the Kuramoto model on the ring graph $C_N(1)$ in the limit $N \to \infty$, the set of zero-mean frequency distributions g for which disorder enhances synchronization has measure zero in the space of distributions. That is, the realization dependence observed in Proposition 3.4 becomes a distributional impossibility in the thermodynamic limit.*

If true, this conjecture would explain the classical intuition that heterogeneity hurts synchronization: for infinite populations, the self-averaging of random frequencies eliminates any beneficial correlations. The finite-N results of Theorem 3.3 would then represent a genuine finite-size effect that vanishes as $N \to \infty$.

5. Conclusion

We have conducted a systematic numerical investigation of disorder-enhanced synchronization in coupled oscillator networks, testing when zero-mean parameter heterogeneity satisfying the barycentric condition [6] can broaden or stabilize synchronization regions. Our main contributions are:

(1) **Stuart–Landau feedforward networks** provide the strongest evidence for disorder-enhanced synchronization: excitation-parameter disorder nearly doubles the phase-locking region (Theorem 3.1), with a monotonic increase in phase-locking fraction from 61% to 100%. The direction of excitation disorder along the feedforward chain determines whether it enhances or suppresses output (Proposition 3.2).
(2) **Kuramoto ring networks** exhibit realization-dependent disorder enhancement: specific zero-mean frequency patterns improve the order parameter by up to 32% (Theorem 3.3), but averaging over random realizations yields a nonsignificant or negative effect (Proposition 3.4).
(3) **The barycentric condition is necessary but not sufficient** for disorder to help (Proposition 3.6). The spectral gap ratio $\rho(G)$ of the graph Laplacian emerges as a predictor of which topologies can benefit (Observation 3.7), and the optimal disorder strength is small (Lemma 3.8).
(4) **The fraction of circulant graphs** benefiting from disorder ranges from 20% to 37% for $N \in \{6, 8, 10\}$ (Theorem 3.5), consistent with the AISync predictions of [10].

These results demonstrate that disorder-enhanced synchronization is a genuine but highly structured phenomenon. Beneficial disorder is not random: it must be aligned with the network topology in specific ways. This structural requirement limits the practical applicability of "disorder as a design tool," but also opens the possibility of deliberately engineering heterogeneity patterns for targeted synchronization enhancement—a direction that warrants both further theoretical analysis (Conjectures 4.1–4.3) and experimental validation with physical oscillator networks.

References

1. Juan A. Acebrón, Luis L. Bonilla, Conrad J. Pérez Vicente, Félix Ritort, and Renato Spigler, *The Kuramoto model: a simple paradigm for synchronization phenomena*, Rev. Modern Phys. **77** (2005), 137–185.
2. Najmeh Ahmed, Thomas Cameron, Antonio Palacios, Jianbo Qi, and Jyoti K. Sahoo, *Effects of heterogeneity in two-cell feedforward networks*, 2026.
3. Florian Dörfler and Francesco Bullo, *Synchronization in complex networks of phase oscillators: a survey*, Automatica **50** (2014), no. 6, 1539–1564.
4. Yoshiki Kuramoto, *Chemical oscillations, waves, and turbulence*, Springer Ser. Synergetics, vol. 19, Springer-Verlag, Berlin, 1984.
5. Ferenc Molnar, Takashi Nishikawa, and Adilson E. Motter, *Network experiment demonstrates converse symmetry breaking*, Nature Phys. **16** (2020), 351–356.
6. Antonio Palacios, Visarath In, and Aric Amani, *Disorder-induced dynamics in complex networks*, Internat. J. Bifur. Chaos Appl. Sci. Engrg. **34** (2024), no. 05, 2430010.
7. Louis M. Pecora and Thomas L. Carroll, *Master stability functions for synchronized coupled systems*, Phys. Rev. Lett. **80** (1998), no. 10, 2109–2112.
8. Arkady Pikovsky, Michael Rosenblum, and Jürgen Kurths, *Synchronization: A universal concept in nonlinear sciences*, Cambridge Univ. Press, Cambridge, 2001.

9. Steven H. Strogatz, *From Kuramoto to Crawford: exploring the onset of synchronization in populations of coupled oscillators*, vol. 143, 2000.
10. Yuanzhao Zhang, Takashi Nishikawa, and Adilson E. Motter, *Asymmetry-induced synchronization in oscillator networks*, Phys. Rev. E **95** (2017), 062215.

Department of Mathematics